Experiments in Fluids 25 (1998) 392–400

Transient temperature measurements in a convectively cooled droplet

C. D. Richards, R. F. Richards

Abstract The transient cooling of an evaporating water droplet, suspended in a jet of dry air, was experimentally investigated in this study using thermochromic liquid crystal thermography. Microencapsulated beads of thermochromic liquid crystals, suspended in the water droplets, enabled the visualization of the transient temperature fields within the droplets. Digital movies of the convectively cooled droplets reveal spatial and temporal temperature gradients resolved down to length scales of ~100 μm and time scales of ~0.03 s. The transient temperature measurements were analyzed to yield total droplet convective heat transfer rates. Droplet heat transfer rates determined from a heat balance on the droplets compare favorably to previously published measurements.

List of symbols

Ψ_∞	free stream relative humidity
A	cross sectional area of the capillary (m^2)
A_s	surface area of droplet
C_p	constant pressure specific heat (kJ/kg K) of water
D	droplet diameter (m)
D_v	mass diffusion coefficient (m^2/s)
e	uncertainty in individual TLC bead temperature
ε	emmissivity
h_c	heat transfer coefficient (W/m^2 K)
h_{fg}	enthalpy of vaporization for water (kJ/kg K)
h_m	mass transfer coefficient (m/s)
HSI	Hue, Saturation, Intensity
k	thermal conductivity of air (W/mK)
Le	Lewis number
m	mass fraction of water in the free stream
m_∞	mass fraction of water vapor in the ambient air
m_s	mass fraction of water vapor at the droplet surface
Nu	Nusselt number
P_{H_2O}	partial pressure of water vapor (kPa)
Pr	Prandtl number
P_{sat}	saturation pressure (kPa)
P_{tot}	total pressure (kPa)
ρ	density (kg/m^3)
r	radial coordinate
R	radius of droplet
Re	Reynolds number
RGB	Red, Green, Blue
rh	relative humidity
σ	Stephan–Boltzman constant
Sc	Schmidt number
Sh	Sherwood number
T	temperature in the free stream (°C)
t	time (s)
T_∞	ambient temperature (C)
T_j	average temperature of ring j
TLC	thermochromic liquid crystals
T_s	surface temperature of droplet (C)
T_v	volume average temperature
V_{drop}	volume of the droplet
V_j	volume of ring j

Received: 11 June 1997/Accepted: 26 March 1998

C. D. Richards, R. F. Richards
School of Mechanical and Materials Engineering
Washington State University
PO Box 642920
Pullman, Washington, USA

Correspondence to: R. F. Richards

This work was supported in part by Washington State University and by the National Science Foundation CTS-9457108.

1 Introduction

The rate of heat transfer to droplets in sprays is a critical issue in the design of many practical spray systems. The control of such diverse processes as spray combustion, spray drying of agricultural products, and spray casting of metals depends on a knowledge of the heat transfer rates to the atomized droplets of evaporating fuel or milk, or solidifying liquid metal. Yet despite much attention, the measurement of heat transfer to droplets in sprays continues to be a challenging problem.

The major stumbling block in determining droplet heat transfer is the lack of a suitable means to measure transient droplet temperatures during the heat transfer process. As a result, most heat transfer correlation's available in the literature have been based on the observation of vaporizing droplets rather than direct measurements of temperature. The first of these experiments were reported by Ranz and Marshall (1952), in which water droplets were suspended in a jet of dry air, on fine-wire thermocouples. The mass flux from the evaporating droplets was determined from sequential size measurements of backlighted photographs of the shrinking droplets. Performing a heat balance on the droplets yielded the heat transfer rate to the droplets and a Nusselt–Reynolds number correlation. Variations on these experiments have been performed on either suspended droplets (Charlesworth and Marshall 1959; Trommelen and Crosby 1970; Yearling and

Gould 1995) or on a linear array of droplets (Nishiwaki 1955). Charlesworth and Marshall (1959) used micro-thermocouples imbedded in the drop to measure the droplet temperature, while the vaporization rate of suspended droplets was deduced from weight changes in the droplets as measured by a sensitive balance.

Yao and Schrock (1976) determined heat transfer rates for freely falling droplets by measuring the temperatures of the droplets before and after they fell. Droplet temperatures were found with one thermocouple placed in the droplet generator and a second thermocouple placed in a small Dewar into which the droplet fell. An energy balance on the droplets yielded the droplet heat transfer. Moresco and Marschall (1979) conducted a similar experiment, but instead of collecting the droplets in a small Dewar, they placed a fine-wire thermocouple in the path of the droplets. Moresco and Marschall were able to extract both mean and surface temperatures for the droplets as they impacted on the thermocouple by measuring the transient thermocouple's signal.

Recently, efforts to overcome the difficulties involved in determining droplet temperatures have resulted in a variety of new techniques in droplet thermography. Optical techniques have held out the most promise for nonintrusive measurements of droplet temperature. Two-color pyrometry has been used to measure the temperature of falling drops of molten metal in an evacuated drop tower (Hofmeister et al. 1989). However, the technique is not practicable at temperatures below about 600 °C. Melton and coworkers have developed a temperature measurement technique based on laser induced exiplex fluorescence (Melton et al. 1986; Wells and Melton 1990), and used it to measure the temperature of drops in free fall. More recently the use of liquid crystal thermography as a means to measure droplet temperatures has been reported by several groups, Hu et al. (1994), Nozaki et al. (1995), Peterson et al. (1995), Treuner et al. (1995), and Richards and Richards (1997).

Thermochromic liquid crystals (TLC) have already been employed in a wide variety of heat transfer experiments, and shown to be a versatile and accurate means of temperature measurement (Akino 1989; D'abiri 1992; Ozawa et al. 1992). Farina et al. (1993) demonstrated that with careful control of the disposition of the TLC material, illumination, and photographic or video recording of the TLC color play, temperature measurements with uncertainties of ± 0.25 K (95% confidence intervals) are possible. Thermochromic liquid crystals can be used in two forms: in their pure form (neat liquid crystals) or in the micro-encapsulated form, where the TLC is encapsulated in hollow, thin-walled plastic beads ranging in diameter from 5 to 3000 μm. Neutrally buoyant microencapsulated beads can be formulated and suspended in a fluid to act as tracer particles that follow the fluid flow.

The use of neat liquid crystals in droplet heat transfer studies has been reported by Hu et al. (1994) and Peterson et al. (1995). Peterson et al. suspended droplets of neat liquid crystal from a micro-thermocouple and recorded their color play with an RGB (red–green–blue) video camera. Hu et al. atomized neat TLC and photographed the droplets in flight using a 35 mm camera.

The use of the microencapsulated form of TLC in droplet thermography has been reported by Nozaki et al. (1995), Treuner et al. (1995), and Richards and Richards (1997). Nozaki et al. used microencapsulated beads to resolve transient temperature fields within water droplets as their buoyancy carried them up through hot, silicone oil. A color video camera recorded the transient temperature field in the water droplets as they convected through the immiscible oil. The droplets studied ranged in size from 2.9 to 8.2 mm in diameter. Treuner et al. used microencapsulated TLC beads to resolve transient temperatures within liquid droplets held between two opposed tubes. A temperature gradient was applied between the opposed tubes and the thermocapillary flow in the droplets imaged under microgravity conditions. These droplets were studied in a glycerol/water solution and had diameters in the range of 13–15 mm. Richards and Richards imaged a 960 μm water droplet suspended from a slender glass capillary. An RGB video camera recorded the color play of 15 μm microencapsulated beads of TLC suspended in the water droplet as the droplet cooled in dry air. The sequence of images of the droplet reveals the transient temperature field in a slice through the center of the droplet.

In the present work, liquid crystal thermography is extended to address heat transfer issues relevant to practical spray devices. The use of the microencapsulated TLC's is applied to the investigation of the transient cooling of very small droplets (diameters less than 1000 μm), in order to map temperature fields and determine transfer rates for the cooling droplets. Video images of convectively cooled water droplets suspended in a jet of dry air are acquired to document the transient temperature fields in the droplets. The images reveal both temporal and spatial temperature gradients within the cooling droplets with resolution down to $\sim$100 μm and $\sim$0.03 s. The transient temperature data are then analyzed to yield convective heat transfer rates for the droplet.

2 Experiment

2.1 Experimental facility

The experiments were conducted in a facility designed to allow video imaging of suspended droplets exposed to precisely controlled convective conditions. Droplets consisting of dilute suspensions of microencapsulated TLC beads in distilled water were hung from a capillary tube in the potential core flow of a vertically oriented jet. A step change in temperature was introduced to the air flow to heat the TLC beads within the droplets above their clearing point. The heating source was then removed and video images were acquired as the droplets cooled. A schematic of the experimental facility is shown in Fig. 1.

The microencapsulated liquid crystal used in all experiments was Hallcrest R30C5W with a nominal color-play range from 30 °C to 35 °C. The beads ranged in diameter from 5 to 15 μm, and were neutrally buoyant in water. The droplets under study were formed of a dilute suspension of the beads of microencapsulated TLC in distilled water. The dilute suspensions were made by mixing the beads in distilled water with concentrations of beads in water of 0.1% on a volume basis.

Droplets with nominal diameters of 1 mm were hung from a Pyrex capillary tube with an OD of 80 μm and an ID of 40 μm.

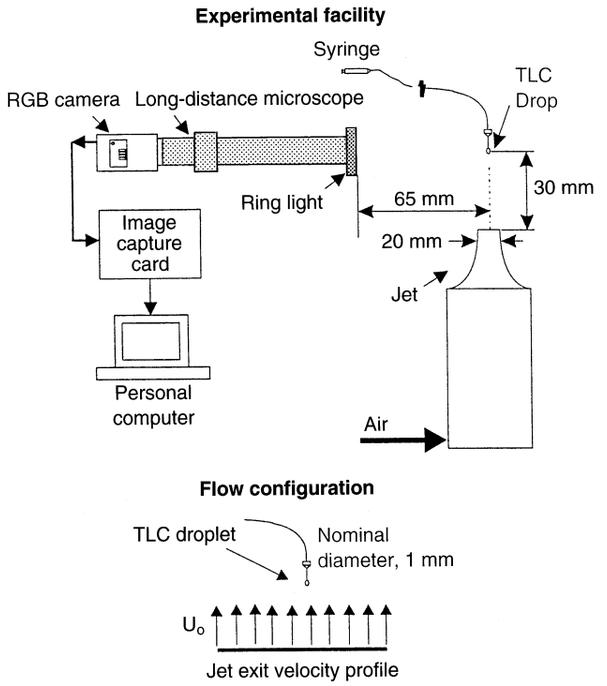

Fig. 1. Schematic of experimental facility

The capillary was bonded to a 24 gauge stainless steel needle with epoxy. The needle was coupled to a Teflon delivery tube using a Luer-Lok fitting. A syringe filled with the dilute suspension of distilled water and microencapsulated TLC was connected to the other end of the delivery tube. Droplets were formed by forcing a small amount of the dilute suspension from the syringe, throughout the delivery tube and out the end of the capillary tube. The syringe provided control over the delivery and size of the droplets. The needle and capillary assembly were fastened to a three-axis micro-positioning device for accurate positioning of the droplet in the potential core of the jet.

An axisymmetric air jet was produced by a nozzle with an ID of 20 mm and a contraction ratio of 9. The inner nozzle contour is a fitted cubic. The contraction is preceded by a flow straightening and conditioning section consisting of honeycomb and screens. Hot-wire anemometry was used to quantify the jet flow produced. Measurements showed that 'top hat' velocity profiles were produced at the jet exit with low turbulence intensity levels (<0.5%). A regulated compressed air source was used to supply the jet flow. The flowrate was monitored using a rotameter calibrated against hot-wire measurements. The air was filtered to remove moisture and particulate matter. Dry and wet-bulb thermometers were used to monitor the jet air temperature and relative humidity.

The jet exit velocity was varied from 0 to 2 m/s in the experiments which resulted in Reynolds numbers of 0 to 2666 based on the jet diameter. Droplet diameters were nominally 1 mm which resulted in droplet Reynolds numbers of 0 to 133. The upper range of Reynolds numbers was restricted because excessive vibration of the droplets (due to vortex shedding) made imaging difficult.

Transient heat transfer experiments were run by suspending a droplet in the potential core of the jet flow and then introducing a step change in temperature to the air flow. This was done by inserting a heated coil of resistance wire (24 gauge Nickel–Chromium wire) briefly into the jet flow upstream of the droplet. The droplets were heated well above the TLC upper event temperature with this method. The elapsed time between removal of the heated wire and the onset of data acquisition was on the order of 2 s which was sufficient to ensure that any flow disturbances introduced by the presence of the wire had been convected downstream of the droplet.

A computer based digital image acquisition system was used to obtain images of the cooling droplets. The system consisted of a long-distance microscope, a CCD camera, an image capturing card, and a personal computer (PC). A schematic of the imaging system is provided in Fig. 1.

The color Hitachi VK-C370 CCD RGB camera acquired RGB signals at 30 frames per second. An Infinity K2 long-distance microscope provided sufficient magnification to resolve individual beads of micro-encapsulated TLC in the water droplets. The spatial resolution of the optics was 2 μm at a stand-off distance of 120 mm. In all experiments the focal plane of the microscope was directed to the center-plane of the droplets. Since the depth of field of the microscope was approximately 100 μm, the resulting images were of 100 μm slices through the center-plane of the droplets. On-axis lighting was supplied by a fiber optic ring light mounted to the microscope. The camera and microscope were mounted on three-axis micro-positioners.

The 30 Hz video RGB output from the camera was received by an IC-PCI/AM-CLR image capturing card from Imaging Technology, Inc. The image capturing card was capable of digitizing 24-bit RGB signals (8 bits for each channel) at a rate of 30 Hz as movies or as individual snapshot images. Digitized images were then sent to a PC with a Pentium 90 MHz processor and 72 MB of RAM for image viewing, processing, analysis, and storage. The expanded RAM in the PC allowed over 40 frames of digitized RGB images (640 × 480 pixels) to be saved. Thus, transient events with durations of up to 1.5 s could be recorded.

2.2 Image processing

Experimental results were stored as uncompressed Audio Video Interleave (AVI) files. In this form, frames could be viewed in sequence as a movie. In addition, each frame was saved in the Tag Image File Format (TIFF) format for individual processing. The time between successive frames is 1/30 of a second.

The first step in image processing was to manually tag each TLC bead in the droplet image. The tagged images were then digitally processed using software developed in-house to yield bead locations and hue values within the droplet.

The Red, Green, and Blue (RGB) values associated with each pixel in an image were transformed into Hue, Saturation, and Intensity (HSI) values. This change from RGB to HSI values is, in essence, a transformation from a Cartesian to a cylindrical coordinate representation of color space. The transformation, given by Gonzalez and Woods (1992), is

$$H = \cos^{-1}\left\{\frac{0.5(\bar{R}-\bar{G})+(\bar{R}-\bar{B})]}{[(\bar{R}-\bar{G})^2+(\bar{R}-\bar{B})(\bar{G}-\bar{B})]^{1/2}}\right\} \quad (1)$$

$$S = 1 - \frac{3}{(\bar{R} - \bar{G} + \bar{B})} \min(\bar{R}, \bar{G} + \bar{B}) \quad (2)$$

$$I = \frac{1}{3}(\bar{R} + \bar{G} + \bar{B}) \quad (3)$$

where $\bar{R}$, $\bar{G}$, and $\bar{B}$ are given by

$$\bar{R} = R/255, \qquad \bar{G} = G/255, \qquad \bar{B} = B/255 \quad (4)$$

and thus values of saturation and intensity are between 0 and 1. Equation (1) yields a value of hue in the interval $0^\circ \leqslant H \leqslant 180^\circ$. When $B/I > G/I$, then H is greater than 180 and the hue was set to $H = 360^\circ - H$ (Gonzalez and Woods, 1992). Hue was then converted to temperature using an experimentally derived calibration relationship.

The entire movie was processed in this manner to yield a series of files containing point measurements of temperature within a droplet as a function of time. From this information contour maps of temperature within a droplet at a specific time were made. In addition, the change of droplet temperature with time was analyzed to obtain heat transfer rates. The specific details of these analyses are provided in the results and discussion.

2.3
Calibration facility and procedure

A relationship between the hue and temperature was developed experimentally. The calibration was conducted in a quiescent chamber in which both temperature and humidity were controlled and monitored. The chamber has optical access for the imaging system described above. The chamber is described in detail in Peterson et al. (1996). Droplets produced from the same suspensions used in the experiments were suspended from capillaries and inserted into the chamber. The chamber was then heated above the clearing point temperature of the TLC. The air in the chamber was humidified by the introduction of steam. During a calibration run the chamber was allowed to slowly cool to ambient temperature at a rate of $-0.2\,^\circ$C per minute. Wet and dry-bulb thermometers placed in close proximity (within 1 cm) to the suspended droplet were used to monitor the temperature and humidity. Calibration measurements were made only when the air in the chamber was saturated (100% rh). The chamber was considered saturated when the wet and dry-bulb temperatures were within $0.2\,^\circ$C (expected thermocouple uncertainty) of each other. Images were acquired every 2 1/2 min (or $0.5\,^\circ$C) as the droplet cooled from $36.0\,^\circ$C to $29.0\,^\circ$C. The acquired images were digitized and processed to yield the hues of individual TLC beads in the isothermal droplets. A hue-temperature calibration curve was drawn by plotting the average individual TLC bead hue against the droplet temperature. Droplet temperature was taken to be equal to the wet-bulb temperature measured in the calibration chamber.

3
Results and discussion

3.1
Calibration

The result of the calibration is shown in Fig. 2. In the figure the temperature of a slowly cooling isothermal droplet is plotted against the average hue of the TLC beads in the droplet. Error bars for each datum indicate the uncertainty in the measured droplet temperature ($0.2\,^\circ$C) and in the average measured TLC bead hue (10°). The solid curve faired through the data indicates a best fit of a cubic equation to the measurements. The dotted lines on either side of the curve indicate a 95% confidence interval on the curve fit. The order of the polynomial used for the curve fit had no physical significance, and was chosen simply to facilitate subsequent analysis of measurements. The calibration curve of droplet temperature versus average TLC bead hue is seen to be a well behaved, monotonically increasing function, with a narrow uncertainty band.

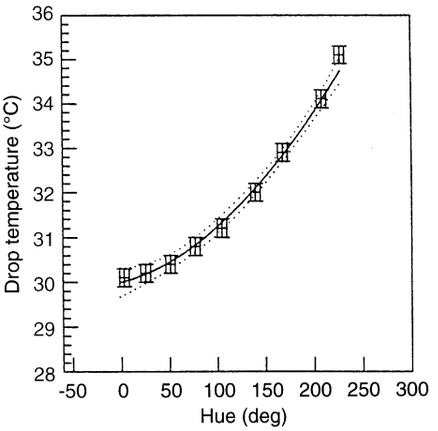

Fig. 2. Calibration curve for thermochromic liquid crystal

The presence of chromatic aberration due to the refraction of light within the droplet is problematic for a measurement technique based on the quantification of hues within a droplet. Since the magnitude of the refraction of the light reaching and reflected from an individual TLC bead depends only on the radial position of the bead, the effect of refraction on measured bead hues was assessed by investigating the dependence of TLC bead hue on the bead's radial position. Figure 3 shows the result of this investigation. In the figure the hue of individual TLC beads, in isothermal droplets at three different temperatures, is plotted against the radial position of the beads. The mean hue values for each droplet are indicated by dashed lines on the figure. The figure clearly demonstrates that the hue of TLC beads throughout the droplets was uniform, as expected for isothermal droplets. Therefore the hue of the beads was unaffected by their radial position in the droplets, and, by chromatic aberration.

3.2
Droplet temperature field

A sequence of three images taken from a movie made of a cooling-droplet is given in Fig. 4. Since the long-distance microscope was focused on the center of the droplet, the images show a view of a 100 μm slice through the center-plane of the droplet. Images in the figure have been taken from odd numbered frames in the movie sequence so that the elapsed time between images is 1/15 of a second. The diameter of the droplet is 960 μm and the Reynolds number (based on the droplet diameter) is 16. The dry and wet-bulb temperatures of the jet air were $20\,^\circ$C and $8\,^\circ$C, respectively.

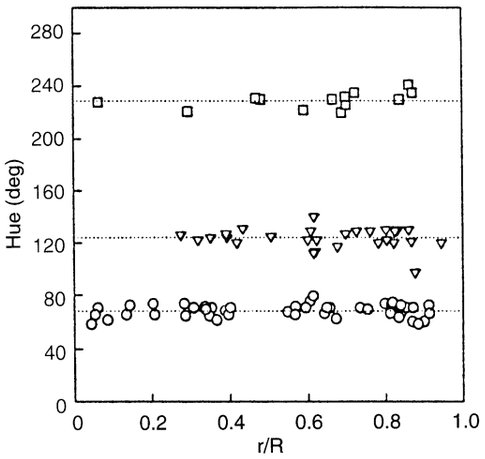

Fig. 3. Hue versus radius for isothermal droplets

The bright circle seen in the images is the reflection of the illuminating ring light. The small patches of color in the images are the individual TLC beads suspended in the droplet. Red TLC bead colors correspond to the lower end of the color play region (30.0 °C) and blue TLC beads correspond to the upper end of the color play region (35 °C). The temperature gradient in the droplet can be identified by the variation of TLC bead color in each of the images. The propagation of the transient cooling process is evident in the sequence of raw images. In the final frame shown only a portion of the droplet temperature remains within the color play range of the TLC beads.

To provide a quantitative record of the transient cooling process of the droplet, contours of constant temperature (isotherms) for the image of the droplet are shown adjacent to the droplet image. The process of mapping the isotherms involves first determining individual TLC bead temperatures, then averaging individual bead temperatures to define the temperature field across the droplet image, and finally using the averaged temperature field to draw isotherms.

To determine individual TLC bead temperatures, hues of the individual TLC beads seen in the images were sampled. In each bead, the value of hue averaged over nine pixels was taken to be the bead hue. Individual TLC bead temperatures were then determined from the bead hues using the calibration curve represented in Fig. 2. The uncertainty in the individual TLC bead temperatures determined in this way is taken to be 0.3 °C based on the variation in hue seen in the isothermal droplets in the calibration runs, and the uncertainty in the fitted calibration curve in Fig. 2.

Figure 5a shows individual TLC bead temperatures measured for the droplet image in Fig. 4a. In the figure the individual bead temperatures are plotted against the bead locations in the image. Bead location is given in terms of pixel location in the image. The scatter seen in the individual bead temperatures in Fig. 5 is due to two effects. First, TLC beads resolved in the droplet image in Fig. 4a may be anywhere throughout the 100 μm depth of field of the long-distance microscope. For example, in the droplet image (a 2D projection), two beads which appear next to each other may in fact be 100 μm apart. Second, there is the scatter in the hues measured in individual TLC beads which contributes to the estimated 0.3 °C uncertainty in the individual TLC bead temperature measurements (discussed above).

It is important to note that bead positions in Fig. 5a have not been corrected for refraction effects. As a result, there is a direct correspondence between the images shown and the contour plots. The effect of refraction is to bend the light reflected from a TLC bead so as to cause the apparent position of the bead seen in the images to be shifted away from the bead's true position. The amount of apparent shift in any given TLC bead's position can be determined from geometric optics, with a simple ray tracing process. The shift in apparent bead position can be shown to be a maximum for beads at radial positions of two-thirds of the total droplet radius. There is no apparent shift in the position of beads at the center of the droplet and at its outer edge.

An averaging process was employed in order to produce a smooth, continuous map of the droplet image temperature field. First, the droplet image was divided up into smaller subregions. For the present work square subregions 100 μm on a side were chosen. The positions of individual TLC beads, were identified, and the beads sorted according to their

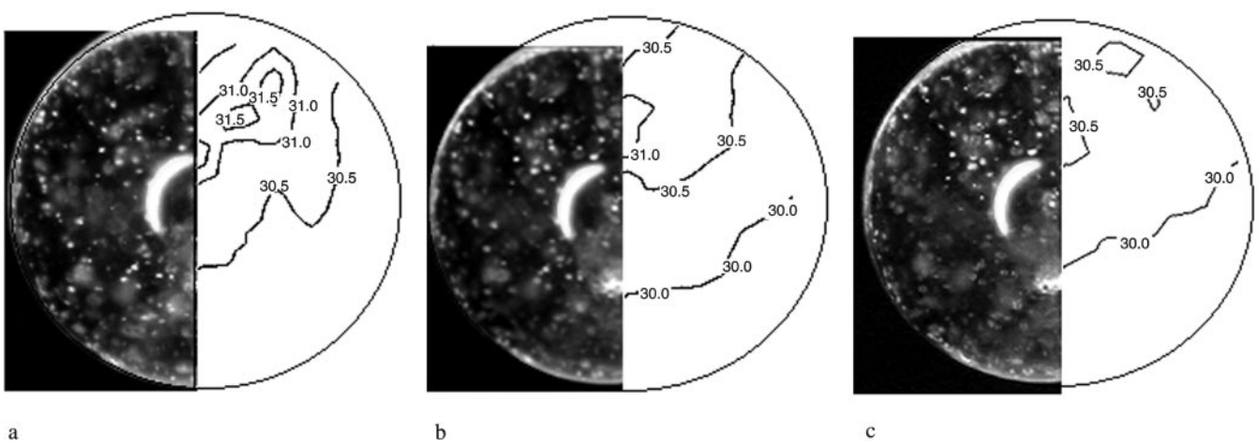

Fig. 4a–c. Images and contours of a cooling droplet

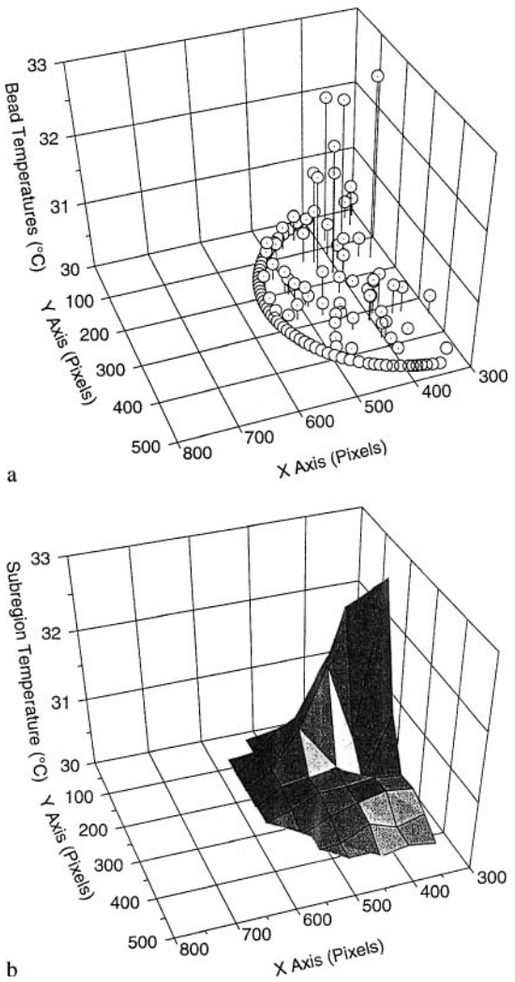

Fig. 5a, b. Droplet temperature measurements. **a** Scatter plot of TLC bead temperatures from Fig. 4a; **b** average subregion temperatures

locations in each of the 100 μm subregions. The measured temperatures of all beads falling in a given subregion were then averaged together to determine the subregion temperature. If a subregion contained two or less TLC beads, then the temperature of the subregion was set to the average temperature of the subregions surrounding it, weighted by the number of beads in each of those subregions. In this way no subregion temperature was determined from an average of less than three individual bead temperatures. The result of subregion averaging of the individual TLC bead temperatures given in Fig. 5a is shown in Fig. 5b. The use of subregion averaging is to smooth out much of the scatter visible in the individual bead temperatures in Fig. 5a.

The uncertainty of the subregion average temperatures can be estimated from $e(N-1)^{-1/2}$. N is the number of individual bead temperatures used in the subregion average and e is the uncertainty of individual bead temperature. Since N is always 3 or larger, taking $N-1=2$ leads to an estimate of the subregion uncertainty of 0.21 °C. However, with such small sample sizes in each subregion, a more conservative estimate of uncertainty, between 0.3 °C (the uncertainty on the individual bead temperature) and 0.2 °C is warranted.

The isotherms seen in Fig. 4a–c are subsequently drawn on the basis of the droplet subregion average temperatures described above. The uncertainty in the temperature contours produced in this way is taken to be equal to the uncertainty of the subregion temperatures on which they are based, or approximately ±0.2 °C to 0.3 °C. The spatial resolution of this method of determining temperature contours is dependent on the size of the subregion chosen for averaging over and on the depth of field of the optics used. The size of the subregion chosen depends both on the density of beads in the droplet images and the depth of field. A higher density of beads allows the use of smaller subregions for the averaging process and finer spatial resolution. A wider depth of field introduces more scatter into the individual bead temperatures sampled in each subregion, and increases the need for larger subregions over which to average. In this work, both the size of the subregion chosen and the depth of field were 100 μm.

The isotherms in Figs. 4a–c quantify the phenomena identified by eye in the droplet images. As the droplet is convectively cooled by air which flows upward from the bottom of the images, the images show the droplet cooling from the bottom, with the isotherms moving upward and inward over time. The temperature difference within the droplet is seen to be as much as one and one half degrees. The temperature contours do not show a fore-aft symmetry. The highest temperatures in the droplet occur off-center, towards the back of the droplet. The location of the high temperature region is stable from frame to frame. In the sequence of images shown, the maximum temperature drops from 31.5 °C to 30.5 °C in an elapsed time of 1/5 of a second. In the first frame all the beads are in the color-play range (i.e., above 30.0 °C), as seen in the contour plot. However as the droplet cools, the 30.0 °C contour progresses up through the droplet, causing those beads below the line to fall below the color-play range of the TLC. In the final frame, the majority of TLC beads in the droplet are below the color-play range.

3.3 Droplet heat transfer

In addition to providing spatially resolved temperature measurements, the experiment provided a means to extract heat transfer information during transient cooling events. Nusselt numbers were calculated for cooling droplets for a range of Reynolds numbers. The results were then compared to the correlation obtained from Ranz and Marshall's (1952) experiments with water droplets evaporating in a laminar jet of dry air.

In order to characterize the temperature of the entire droplet a volume averaging technique was used. The technique parallels the method used to find the square subregion temperatures above. For the volume averaging the droplet image was divided into subregions of concentric rings. Each ring in the 2-d image corresponded to a spherical shell in the 3-d droplet. The temperature of each ring was determined by averaging the temperatures of all TLC beads in the ring. The volume average temperature of the droplet was then determined by averaging the temperatures of each ring in the 2-d droplet image, weighted by the volume of the associated spherical shell of the 3-d droplet. A volume-weighted mean

droplet temperature was calculated from

$$T_v = \sum_{j=1}^{n} T_j \frac{V_j}{V_{\text{drop}}} \tag{5}$$

where T_v is the volume-average temperature, T_j is the average temperature of ring j, V_j is the volume of ring j, and V_{drop} is the volume of the droplet.

A volume-average droplet temperature was determined for each image in a cooling droplet movie. Figure 6 shows a plot of volume average temperature versus time for a typical experiment. In this experiment the droplet was cooled in quiescent air, so that $Re = 0$. The change in temperature of the droplet is seen to be linear, with the temperature of the droplet falling from 32.1 °C to 30.2 °C during an elapsed time of 0.38 s.

Implicit in this procedure is the assumption that the temperature field in the droplet is not highly three dimensional, but is well represented by the two dimensional temperature field in the droplet image. This assumption is supported by the fact that the cooling air flow over the droplet was arranged to produce as nearly as possible a two-dimensional heat transfer problem. In other words, azimuthal variation in the air flow past the droplet and in the heat transfer from the droplet was not expected.

The uncertainty in the volume-average droplet temperature can be estimated in the same way as the uncertainty in the droplet subregion temperatures. The uncertainty of the droplet volume averaged temperatures should be estimated as $(N-1)^{-1/2}$ times the uncertainty of the individual bead temperature uncertainty, where N is the number of individual bead temperatures used in the droplet volume average. Since N was always greater than 50 in the present set of experiments, taking $(N-1) = 49$ leads to an estimate of the uncertainty of less than 0.1 °C.

In Ranz and Marshall's experiments mass transfer rates from evaporating droplets were measured and used to determine the heat transfer to a suspended droplet by invoking a steady-state energy balance. The resulting droplet Nusselt number was found to correlate with droplet Reynolds number and the Prandtl number as:

$$Nu = 2.0 + 0.60 Re^{1/2} Pr^{1/3} \tag{6}$$

Although a comparison will be made to the results of Ranz and Marshall (1952), there were some important differences between the two sets of experiments that should be pointed out. First the time scales of the experiments performed by Ranz and Marshall were relatively long. The time scales in the present set of experiments were very short. Second, the experiments by Ranz and Marshall were steady-state; the temperature of a droplet was constant at the wet-bulb temperature. The present set of experiments were transient, with the droplet temperature constantly decreasing. The droplets never reached the wet-bulb temperature of the air stream. Third, the experiments by Ranz and Marshall were performed by placing a cool droplet in a hot air stream. Under these conditions heat was transferred by conduction into the droplet while latent heat was transported by evaporation out of the droplet. Conduction and evaporation were opposed. The present set of experiments were performed by placing a hot droplet in a cool air stream. Under these conditions both sensible heat and latent heat were transported out of the droplet. Conduction and evaporation acted in the same direction. Finally, Ranz and Marshall's heat transfer measurements were made by determining the change in the mass of the evaporating droplets, and invoking a balance between latent and sensible heat transfer to the droplet. In the present work, the heat transfer measurements were made by determining the change in temperature of the evaporating droplets, and invoking a balance between the latent and sensible heat out of the droplet and the change of enthalpy of the droplet.

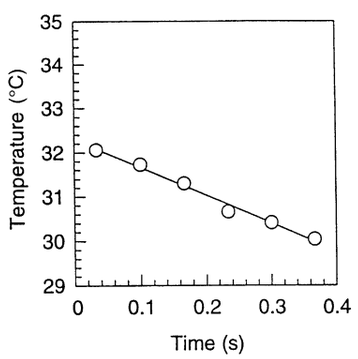

Fig. 6. The change in average droplet temperature over time ($Re = 0$)

In the present experiments then, the heat balance applied to the droplet was

$$mC_p \frac{dT}{dt} = h_c A_s (T_\infty - T_s) + h_m A_s (m_\infty - m_s) h_{fg} + \sigma \varepsilon A (T_\infty^4 - T_s^4) + kA \frac{dT}{dx} \tag{7}$$

where h_c and h_m were the total droplet heat and mass transfer coefficients, C_p and h_{fg}, were the constant pressure specific heat and enthalpy of vaporization for water, k, was the thermal conductivity of glass, and σ was the Stefan–Boltzmann constant. The symbols A_s and m were the surface area and mass of the droplet, and A was the cross-sectional area of the capillary. The driving potentials for heat and mass transfer were T and m the temperature and mass fraction of water vapor in the free stream, and T_s and m_s, the temperature and mass fraction of water vapor at the droplet surface.

The contribution from radiation and conduction along the capillary were small effects and thus were neglected in the analysis. The terms were rearranged to solve explicitly for the Nusselt number by invoking the definition of the Nusselt, Sherwood, and Lewis numbers:

$$Sh = \frac{h_m D}{\rho D_v}, \quad Nu = \frac{h_c D}{k}, \quad Le = \frac{Sc}{Pr} \tag{8}$$

The Nusselt number was then obtained from

$$Nu = \frac{mC_p \dfrac{dT}{dt}}{\dfrac{A_s}{D}\left[\rho D_v Le^{1/3} (m_\infty - m_s) h_{fg} + k(T_\infty - T_s)\right]} \tag{9}$$

where C_p and h_{fg}, were evaluated at the mean droplet temperature. The binary diffusivity of water vapor in air, D_v, and the conductivity, k, and Lewis number, Le, for air were evaluated at the film temperature. Water vapor mass fractions in the free stream and at the droplet surface, m_∞ and m_s, were found from

$$m = \frac{P_{H_2O}}{1.61P_{tot} - 0.61P_{H_2O}} \tag{10}$$

where the water vapor partial pressure $P_{H_2O} = P_{H_2O,\infty}$ in the free stream and $P_{H_2O} = P_{H_2O,s}$ at the droplet surface, respectively. P_{tot} was the total pressure. Water vapor partial pressure in the free stream was determined from the relative humidity

$$P_{H_2O,\infty} = \psi_\infty P_{sat}(T_\infty) \tag{11}$$

where the free stream relative humidity, ψ_∞, was found from the wet and dry-bulb temperatures. The water vapor at the surface of the droplet was taken to be saturated so that the partial pressure there was

$$P_{H_2O,s} = P_{sat}(T_s) \tag{12}$$

The free stream temperature, T_∞ was measured by the dry-bulb thermocouple. The droplet surface temperature, T_s, was more difficult to define for three reasons. First, few beads could be discerned right at the outermost radius of the droplet, so that a direct determination of surface temperature was difficult. Second, the surface temperature of the droplet varied around the circumference of the droplet, from the stagnation point to the attachment point at the glass capillary. Third, the surface temperature varied with time as the entire droplet cooled. A quick inspection of Figs. 4a–c verifies these last two points. The first difficulty was overcome by plotting the temperatures of the TLC beads near the stagnation point of a droplet (in a given image) versus radius, and applying a linear fit to the measured temperatures. The temperature at the stagnation point of the droplet was then found by extrapolating the linear fit to the droplet surface. This method resulted in estimations of the stagnation point temperatures with uncertainties comparable to the uncertainties in subregion average temperatures of around 0.3 °C. Due to the variation in the surface temperature of the droplet around the circumference of the droplet the uncertainty in the surface temperature is higher than this value. For this reason, the uncertainty in droplet surface temperature was taken to be 0.75 °C. Although this uncertainty is large, the sensitivity of droplet Nusselt number on droplet surface temperature is not great, as will be seen later.

The rate of change of the droplet temperature with time, dT/dt, was determined by plotting the volume average temperature of the droplet versus time and then fitting a line to the data points. The slope of this line was taken to be dT/dt. Figure 6 shows a plot of volume average droplet temperature versus time for a typical experiment, and the least squares fit to the data. The change in temperature of the droplet is seen to be linear, with the temperature of the droplet falling from 32.1 °C to 30.2 °C during an elapsed time of 0.38 s giving a slope of −6.1 °C/s. The standard deviations of the slopes determined from linear regression were typically 5% of the estimated slope and always less than 10% of the estimated slope.

Droplet diameter was measured directly from the images. The mass and surface area of the droplet were determined from the measured droplet diameter, assuming a spherical droplet. The droplet seen in Fig. 4 was typical of the droplets used in the experiments, which were all very close to spherical. Uncertainty in determining droplet size from the images was estimated at 5%. Droplet size did not measurably change during the runs, which were never longer than 1.5 s.

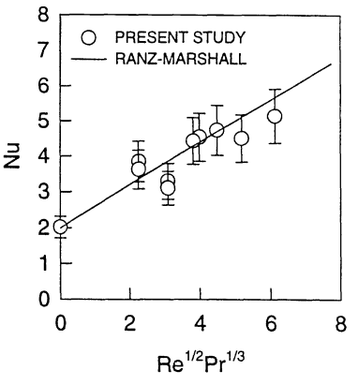

Fig. 7. Heat transfer correlation

The results of the heat transfer measurements are shown in Fig. 7. In the figure, measured Nusselt numbers are plotted against $Re^{1/2}Pr^{1/3}$. Bars on each datum indicate the estimated uncertainty in Nu of 15%, where the uncertainty is determined using the method of Kline and McClintock (1953). The uncertainty in the time derivative of the volume average droplet temperature and the uncertainty in droplet diameter each result in approximately 5% uncertainty in Nu. The droplet surface temperature uncertainty results in a 3.5% uncertainty in Nu, and the thermophysical properties (such as freestream wet and dry-bulb temperatures) contribute approximately 1.5% to the Nu uncertainty. Thus although the uncertainty in the estimate of droplet surface temperature is large, the sensitivity of Nusselt number on droplet surface temperature is not great, so that uncertainty in droplet surface temperature is less significant than the uncertainties in the droplet diameter and the time derivative of the volume-average droplet temperature in determining the final Nusselt number uncertainty. Uncertainties in free stream dry and wet-bulb temperatures, and thermophysical properties are even less significant. The uncertainty in $Re^{1/2}Pr^{1/3}$, which is due primarily to uncertainty in droplet diameter, is small and is comparable to the size of the symbols (open circles) indicating the data.

The heat transfer correlation reported by Ranz and Marshall (1952) is shown with a solid line in the figure. The comparison between the present set of measuremens and the measurements made by Ranz and Marshall is quite good.

4 Conclusions

Thermochromic liquid crystal thermography has been used to study transient temperature events in a convectively-cooled droplet. The work has demonstrated that imaging of individual microencapsulated beads suspended within a droplet can be used successfully to determine heat transfer and temperature information. Both spatially and temporally resolved temperature measurements were acquired in cooling droplets from

Reynolds numbers ranging from 0 to 100. Transient temperature gradients have been imaged in the cooling droplet with resolutions down to ~100 μm and ~0.03 s. Heat transfer rates determined from transient temperature data extracted from the images compare favorably to previous measurements by Ranz and Marshall.

References

Akino N; Kunugi T; Ichimiya K; Mitsushiro K; Ueda M (1989) Improved liquid–crystal thermometry excluding human color sensation. ASME J Heat Transfer 111: 558–565

Charlesworth DH; Marshall WR (1960) Evaporation of drops containing dissolved solids. AIChE 6: 9–23

D'abiri D; Gharib M (1992) Digital particle image thermometry: the method and implementation. Exp Fluids 11: 765–775

Farina DJ; Hacker JM; Moffat RJ; Eaton JK (1993) Illuminant invariant calibration of thermochromic liquid crystals. Visualization of heat transfer processes. HTD-Vol. 252, ASME 29th Nat Heat Transfer Conf, Atlanta, Georgia, pp 1–11

Gonzalez RC; Woods RE (1992) Digital image processing. Addison-Wesley, Reading, MA, pp 229–235

Hofmeister WH; Bayuzick RJ; Robinson MB (1989) Noncontact temperature measurement of a falling drop. Int Thermophys 10: 279–292

Hu SH; Richards RF; Richards CD (1994) Thermography of atomized droplets in flight using thermochromic liquid crystals. ILASS Conf Seattle, WA

Kline SJ; McClintock FA (1953) Describing uncertainties in single sample experiments. Mech Eng 75: 3–8

Melton LA; Murray AM; Verdieck JF (1986) Laser fluorescence measurements in fuel sprays. Soc Photo Opt Instr Eng 664: 40

Moresco LL; Marschall E (1979) Temperature measurements in a liquid–liquid direct-contact heat exchanger. AIChE Symp Ser 75: 266–272

Nishiwaki N (1955) Kinetics of liquid combustion processes: evaporation and ignition lag of fuel droplets. 5th Symp (Int.) on Combustion, pp 148–158

Nozaki T; Mochizuki T; Kaji N; More YH (1995) Application of liquid-crystal thermometry to drop temperature measurements. Exp Fluids 18: 137–144

Ozawa M; Muller U; Kimura I; Takamori T (1992) Flow and temperature measurement of natural convection in a hele-Shaw cell using a thermo-sensitive liquid-crystal tracer. Exp Fluids 12: 213–222

Peterson D; Hu SH; Richards CD; Richards RF (1995) The measurement of droplet temperature using thermochromic liquid crystals. ASME HTD 308: 39–46

Ranz WE; Marshall WR (1992) Evaporation from drops: Part II. Chem Eng Prog 48(4): 173–180

Richards CD; Richards RF (1997) Convective cooling of a suspended water droplet. ASME J Heat Trans 119: 208

Treuner M; Rath HJ; Duda U; Siekmann J (1995) Thermocapillary flow in drops under low gravity analysed by the use of liquid crystals. Exp Fluids 19: 264–273

Trommelen AM; Crosby EJ (1970) Evaporation and drying of drops in superheated vapors. AIChE J 16: 857–867

Wells MR; Melton LA (1990) Temperature measurements of falling droplets. ASME J Heat Transfer 112: 1008–1013

Yao S-C; Schrock VE (1976) Heat and mass transfer from freely falling drops. ASME J Heat Trans 98: 120–126

Yearling PR; Gould RD (1995) Convective heat and mass transfer from single evaporating water, methanol and ethanol droplets. ASME Fluids Engineering Conf, FED-223, pp 33–38